

Communication

Quad-Band Circular Polarized Antenna for GNSS, 5G and WIFI-6E Applications

Xiaoming Liu ^{1,2,3,*}, Haiyang Wang ², Xiaofan Yang ¹ and Jinhong Wang ^{1,4}

¹ The State Key Laboratory of Complex Electromagnetic Environment Effects on Electronic and Information System, Luoyang 471004, China; xiaofan_uestc@sina.com (X.Y.); jhwang@nwpu.edu.cn (J.W.)

² School of Physics and Electronic Information, Anhui Normal University, Wuhu 241002, China; why97@ahnu.edu.cn

³ Wuhu CEPREI Information Industry Technology Research Institute, Wuhu 241002, China

⁴ The School of Marine Science and Technology, Northwestern Polytechnical University, Xi'an 710072, China

* Correspondence: xiaoming.liu@ahnu.edu.cn

Abstract: A quad-band circularly-polarized antenna, for applications of a global navigation satellite system (GNSS), 5G, and WIFI-6E, is designed, fabricated, and measured. The proposed antenna is formed by an L-shaped radiator, a rectangular frame ground with an L-shaped stub, and a rectangular strip at the opposite corner. The microstrip antenna can generate four frequency bands, covering WIFI-6E (5925–7125 MHz), 5G n77 (3300–4200 MHz), n78 (3300–3800 MHz), and the GNSS bands. This antenna generates right hand circular polarization (RHCP) waves in the low frequency band (0.95–2.11 GHz), covering GPS, BDS, GLONASS, and GALILEO applications. Moreover, an L-shaped aperture and three rectangular slits are cut on the ground to broaden the axial-ratio bandwidth at the upper band. A prototype is fabricated and measured to verify the performance of this design. It is shown that the agreement between the simulation and measurement is satisfactorily good. The measured –10 dB bandwidths for each band are 75.8% (0.95–2.11 GHz), 55.8% (3.05–5.39 GHz), 39.9% (5.84–8.19 GHz) and 10.3% (9.14–10.68 GHz), respectively. While the measured 3 dB axial-ratio bandwidths are 59.4% (1.16–2.14 GHz), 35.8% (3.23–4.64 GHz), 8.4% (5.70–6.20 GHz), and 2.6% (7.51–7.71 GHz), the measured gains are 4.56, 2.28, 4.26, and 4.30 dBi at 1.5 GHz, 3.8 GHz, 6 GHz, and 7.6 GHz, respectively.

Keywords: quad-band; circularly polarized; global navigation satellite system; 5G



Citation: Liu, X.; Wang, H.; Yang, X.; Wang, J. Quad-Band Circular Polarized Antenna for GNSS, 5G and WIFI-6E Applications. *Electronics* **2022**, *11*, 1133. <https://doi.org/10.3390/electronics11071133>

Academic Editors: Pavlos Lazaridis, Zaharias Zaharis, Raed A. Abd-Alhameed and Bo Liu

Received: 13 March 2022

Accepted: 31 March 2022

Published: 2 April 2022

Publisher's Note: MDPI stays neutral with regard to jurisdictional claims in published maps and institutional affiliations.



Copyright: © 2022 by the authors. Licensee MDPI, Basel, Switzerland. This article is an open access article distributed under the terms and conditions of the Creative Commons Attribution (CC BY) license (<https://creativecommons.org/licenses/by/4.0/>).

1. Introduction

The circular polarization (CP) antenna is an important component in many communication systems. The investigation into this component has been a hot topic for many years [1,2]. Electromagnetic waves usually encounter reflection and refraction during propagation, which often leads to a change in polarization direction or state [3]. In addition, when travelling through the ionic and rain layers, depolarization effects may occur, which is very harmful to communication links. It is well recognized that a circularly polarized wave is less affected by the Faraday rotation [4,5] in comparison to a linearly polarized one. Moreover, it is superior in countering the depolarization effect. Therefore, circularly polarized antennas are usually used in global navigation satellite systems (GNSS). They also have important applications in various wireless systems, such as radar and mobile communication systems [6].

With the swift development of wireless communication, many functions are integrated into a single terminal device, and multi-band antennas are in active demand. Antennas working over several frequency bands with circularly polarized properties are, therefore, highly preferred. The first requirement may be the coverage of several navigation systems simultaneously; the second requirement is that other wireless communications, such as

5G and WIFI, can be integrated in a single terminal device. In this connection, further investigation into multi-band circularly polarized antennas is required.

For an arbitrary electromagnetic wave, its electric field \vec{E} can be divided into two components, i.e., $\vec{E} = E_x e^{j\varphi_x} \hat{e}_x + E_y e^{j\varphi_y} \hat{e}_y$. If the amplitudes of the two components are equal ($E_x = E_y$) and the phase difference meets $\varphi_y - \varphi_x = \pm 90^\circ$, the resultant field appears as a circularly polarized wave [7]. There are many techniques to realize CP antennas, such as cutting slots [8–10], adding branches [11,12], using a feed network with a phase difference of 90° [13,14], etc. In Ref. [14], a polarization reconfigurable antenna was developed for GNSS. The variation in operation frequency is tuned by PIN-diode switches, which are not multi-band operation antennas. A compact antenna was proposed in Ref. [15], through using two T-coupling lines with different lengths as feeds, to achieve circular polarization. It can fully cover the GPS L1 band. Stacking radiating patches is another common method to generate multi-band circular polarization [16–19]. The main drawbacks of the stacking technique are the difficulty in fabrication and relatively larger thickness, which is not preferred in many mobile terminals. Multi-band circular polarization can also be achieved by etching slots on the ground layer [20–23]. Most of these designs can provide dual-band operation. In Ref. [24], a circularly polarized antenna is developed based on a dielectric resonator. This antenna can excite six different mixed radiation modes and generate four frequency bands for BDS, GPS, WLAN, and WiMAX. However, the axial-ratio (AR) bandwidth is narrow, while the antenna size is relatively large. In Ref. [25], a three-band circularly polarized antenna was proposed. By using a linear-to-circular polarization converter on the bottom layer, circular polarization waves can be radiated. The antenna provides three AR bandwidths of 3.53%, 1.73%, and 13.62%, which are very suitable for satellite applications. However, it does not have extra bands for other wireless communications. In Ref. [26], a tri-band, wearable circularly polarized antenna was proposed, which can be used in WLAN, C band, and X/Ku band. The AR bandwidths of each band are 10.10% (4.7–5.2 GHz), 4.95% (5.9–6.2 GHz), and 10.44% (11.8–13.1 GHz), respectively.

At present, the navigation systems include GPS, BDS, GALILEO, and GLONASS [27,28]. These systems operate at different frequency bands, GPS: L1 (1227.60 ± 10.23 MHz) and L2 (1575.42 ± 10.23 MHz); GALILEO: E1 (1227.60 ± 1.023 MHz) and E5b (1575.42 ± 1.023 MHz); BDS: B1(1561.098 ± 2.046 MHz) and B2 (1207.14 ± 2.046 MHz); GLONASS: L1 (1602.5625 ± 4 MHz) and L2 (1246.4735 ± 4 MHz). These frequency bands are so close to each other that it is best to create one single band where all four of the navigation systems are covered. In addition, to cover other wireless communications, extra frequency bands have to be created. It is, therefore, necessary to develop multiple frequency bands with circularly polarized radiation. Since the development of 5G and WIFI-6E, technology has brought about a substantial increase in data transmission rates as well as shorter network delays [29,30]. An antenna that can match multiple frequency bands of GNSS, 5G, and WIFI 6E will see wide application in a terminal device.

In this communication, a quad-band circularly polarized antenna that can cover almost all global navigation frequency bands is proposed. The antenna is formed by an L-shaped radiator, a rectangular frame ground with an L-shaped stub, and a rectangular strip at the corner. An L-shaped aperture and three rectangular slits were cut on the ground to improve current distribution, which can broaden AR bandwidth at the 5G frequency band. The detailed geometry for the proposed antenna is shown in Section 2. By optimizing parameters, impedance bandwidth and AR bandwidth are further improved. The measured results are shown in Section 5.

2. Structure and Analysis

The geometry of the proposed antenna is schematically shown in Figure 1. The antenna is fed through a $50\ \Omega$ microstrip feedline. The feedline is connected to an L-shaped patch, acting as field excitation and radiator. The L-shaped patch is printed on an FR4 substrate with $\epsilon_r = 4.4$ and $\tan \delta = 0.02$, and the frame ground is fabricated on the bottom of the substrate.

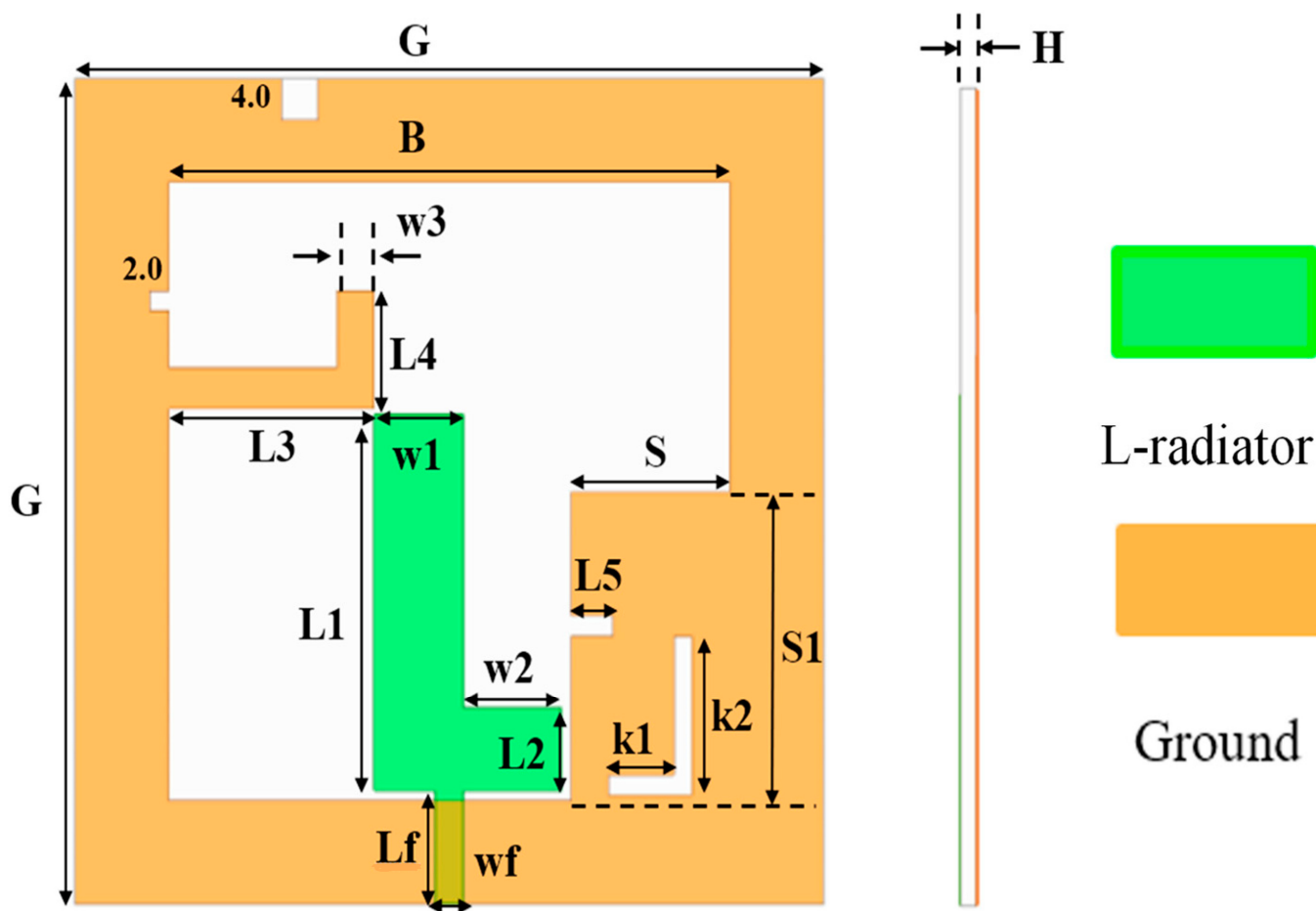


Figure 1. Geometry and parameters of the proposed antenna.

The side length of the substrate is G , and the thickness is H . To assess the performance of this antenna, a commercial solver, ANSYS HFSS, is used for simulation. The resultant values for each parameter are listed in Table 1.

Table 1. Dimension of the proposed antenna.

Parameter	Value/mm	Parameter	Value/mm
G	80	L_f	11
B	60	W_1	9.5
H	1.6	W_2	11.5
L_1	36.5	W_f	3
L_2	8	S	18
L_3	20	S_1	30
L_4	11.5	K_1	8
L_5	5	K_2	15.5

The evolution process is illustrated in Figure 2. A square slot with side lengths of B is introduced in the ground plane, shown as Ant. 1, in Figure 2. An L-shaped stub is then protruded from the left side of the ground plane toward the center, and it is marked as Ant. 2. Following on, a rectangular patch is placed on the bottom right corner of the ground and seen as Ant. 3. At last, four slots are etched on the ground frame and shown as Ant. 4. In order to demonstrate the evolution of the antenna, the AR and impedance bandwidth of each antenna are simulated and plotted in Figure 3.

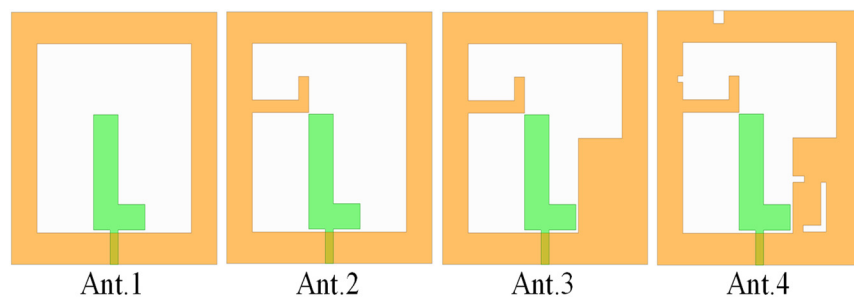


Figure 2. Evolution of the proposed antenna.

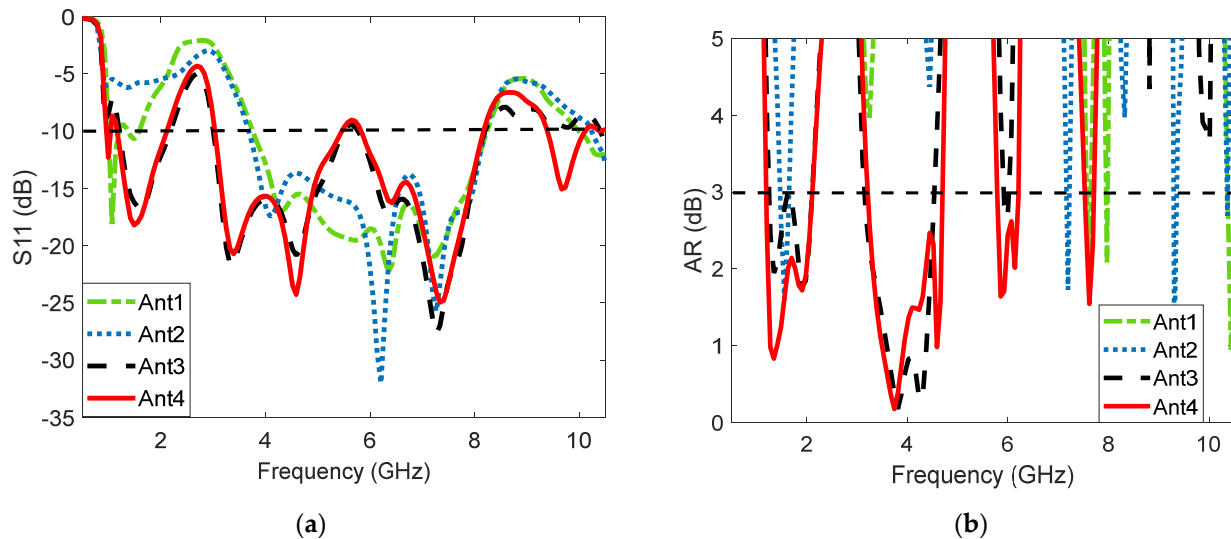


Figure 3. Simulated results for Ant. 1–Ant. 4: (a) S_{11} , (b) AR.

The basic structure is Ant. 1, which has a frame ground and an L-shaped radiator, as used in Ref. [30]. It is seen, from the simulated results, that Ant. 1 provides a wide impedance bandwidth in the range of 3.8–8.2 GHz. However, it is linearly polarized in this operation range. Even worse, the impedance matching is not good enough in the navigation bands. To improve the quality of circular polarization, an L-shaped branch is added to the upper left corner, as shown with Ant. 2 in Figure 2. Although the impedance bandwidth becomes worse in the low frequency around 1.5 GHz, the axial ratio is greatly improved. To create resonance in the navigation bands, a rectangular patch is placed at the lower right corner of the ground plane, as seen with Ant. 3. Apparently, the impedance bandwidth and axial ratio have been greatly improved. Therefore, the rectangular patch can improve impedance matching at lower and upper bands. By adding slots on the ground plane, the AR may be further improved, as seen with Ant. 4. The bandwidth does not see significant change, while the AR is greatly improved—particularly at 1–2 GHz and around 6 GHz.

3. Parametric Study

To examine the sensitivity of each parameter, a systematic study has been conducted. The purpose of doing this is to find the fabrication tolerance and, more importantly, to pinpoint the effects of these parameters on AR and bandwidth. We have chosen four parameters, i.e., the length of the L-shaped radiator L_1 , the L-shaped branch length L_4 , the width of the rectangular patch S , and the width of the narrow feeding line connecting to the coaxial cable. The first three parameters correspond to the evolution process, and the last parameter is chosen because it determines the input impedance, and therefore, in most cases, it is the most sensitive parameter.

The L-shaped patch acts as field excitation and a radiator. Letting $L_1 = 35.5, 36.5$, and 37.5 mm, it is found that the reflection coefficients for these cases do not see significant

variation, as shown in Figure 4. Only a slight change takes place in the 10 GHz band. For the axial ratio, the change occurs in the 7.6 GHz band. The criterium of -3 dB is not met for $L_1 = 37.5$ mm. For the L-shaped branch, when changing the length, it is also found that the reflection coefficients do not change significantly, as shown in Figure 5. In addition, the axial ratio sees apparent change in the 4 GHz and 7.6 GHz bands. It is seen from Figure 6 that the width of the patch S does produce some effect on the reflection coefficients. However, the -10 dB bandwidths for each band do not change significantly. Its effect on the axial ratio happens in all four of the bands—particularly for the 4 GHz, 6 GHz, and 7.6 GHz bands.

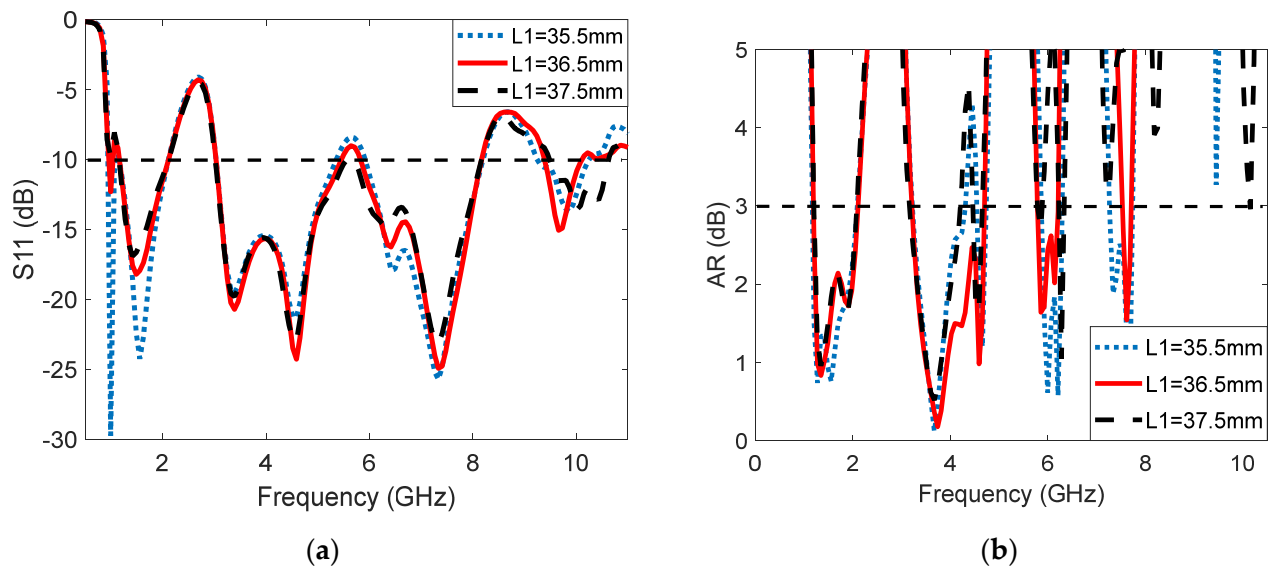


Figure 4. Effect of L_1 on antenna performance: (a) S_{11} , (b) AR.

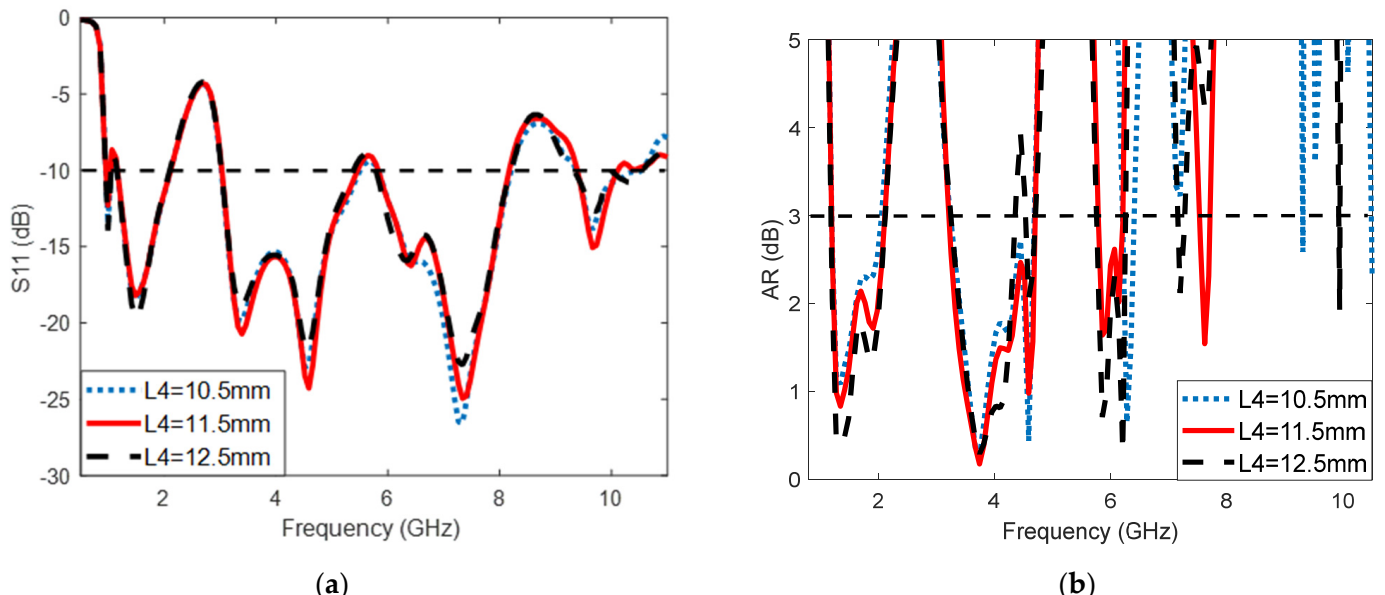


Figure 5. Effect of L_4 on antenna performance: (a) S_{11} , (b) AR.

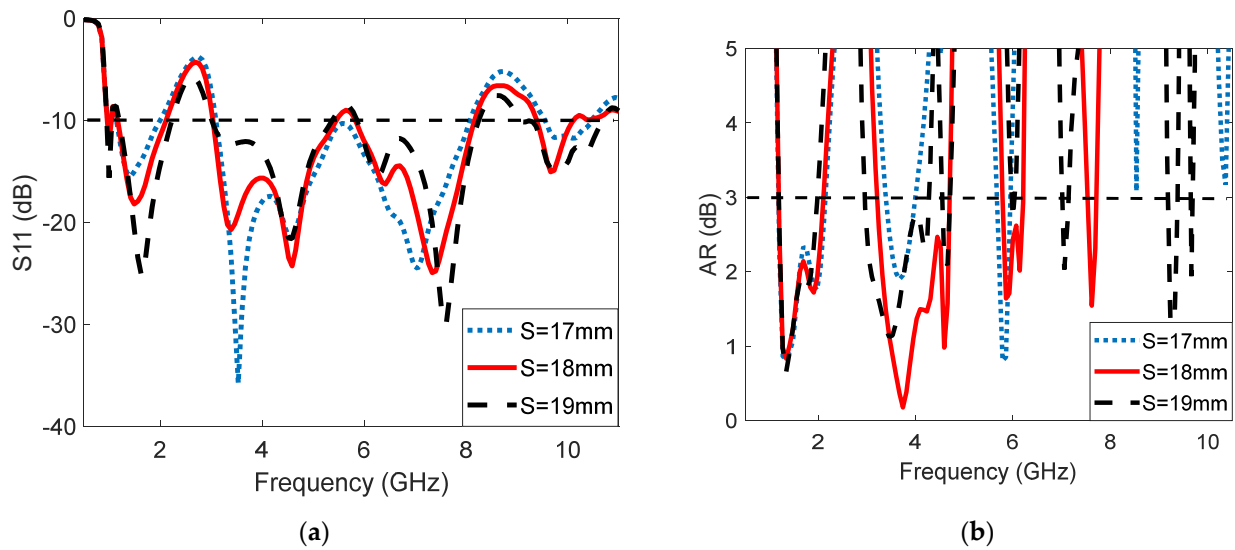


Figure 6. Effect of S on antenna performance: (a) S_{11} , (b) AR.

The last parameter, wf , is the width of the feed. It is clearly seen from Figure 7 that the change in the width affects the reflection coefficients considerably. In other words, the impedance matching varies significantly with the change in wf . For the axial ratio, the change is much greater for the higher frequency bands than the lower frequency bands. It appears that the 4 GHz and 7.6 GHz bands are more sensitive to changes in the parameters.

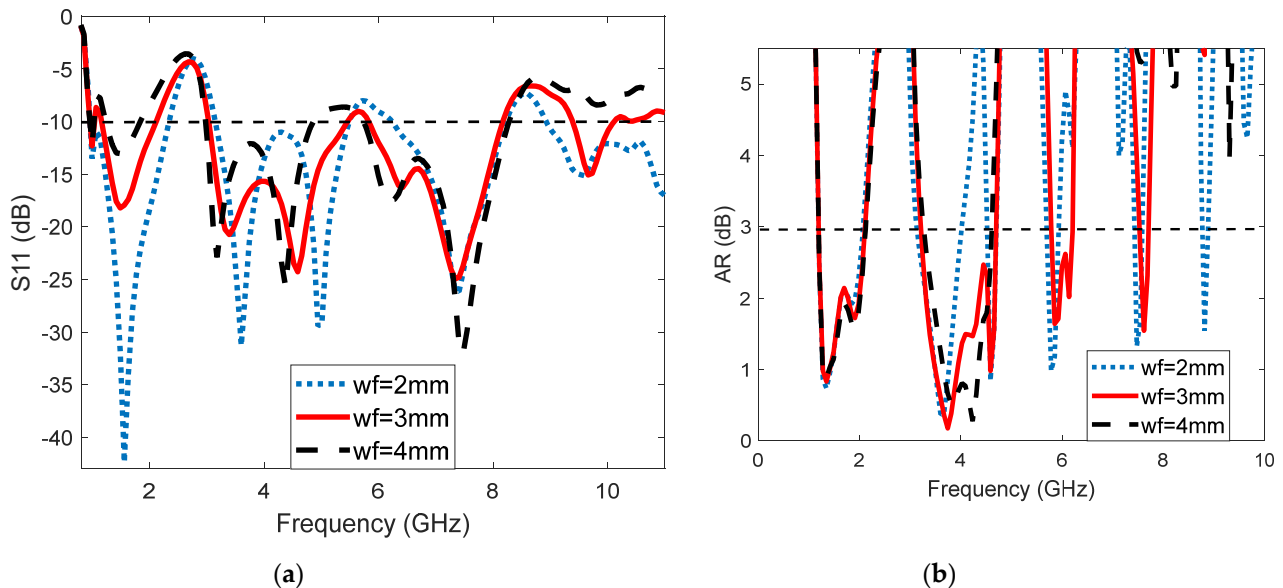


Figure 7. Effect of wf on antenna performance: (a) S_{11} , (b) AR.

It is seen, from the parametric study, that the most sensitive parameter on the impedance bandwidth is the width of the feedline wf . The width of the patch S also produces some effect on the impedance bandwidth. Other parameters have very limited effects on the impedance bandwidth. In comparison, the width of the patch S produces a considerable effect on the AR bandwidth. While the width of the feedline wf produces some effect on the AR bandwidth, other parameters have fewer effects on the AR bandwidth.

4. Currents Distribution

In order to shed more light on the process of generating circular polarization and determining the direction of the circular polarization, the surface current distributions are

shown in Figure 8, where Figure 8a shows the current distributions of 0° , 90° , 180° , and 270° at 1.5 GHz. From the plot, it is seen that currents rotate, in the counterclockwise sense, as the phase increases, which means that the antenna radiates right-handed circularly polarized (RHCP) waves at low frequency bands. In addition, the current is distributed over the frame ground, indicating that the frame also functions as a radiator at 1.5 GHz. It has to be mentioned that most navigation satellite transmitting antennas are right-handed circularly polarized antennas.

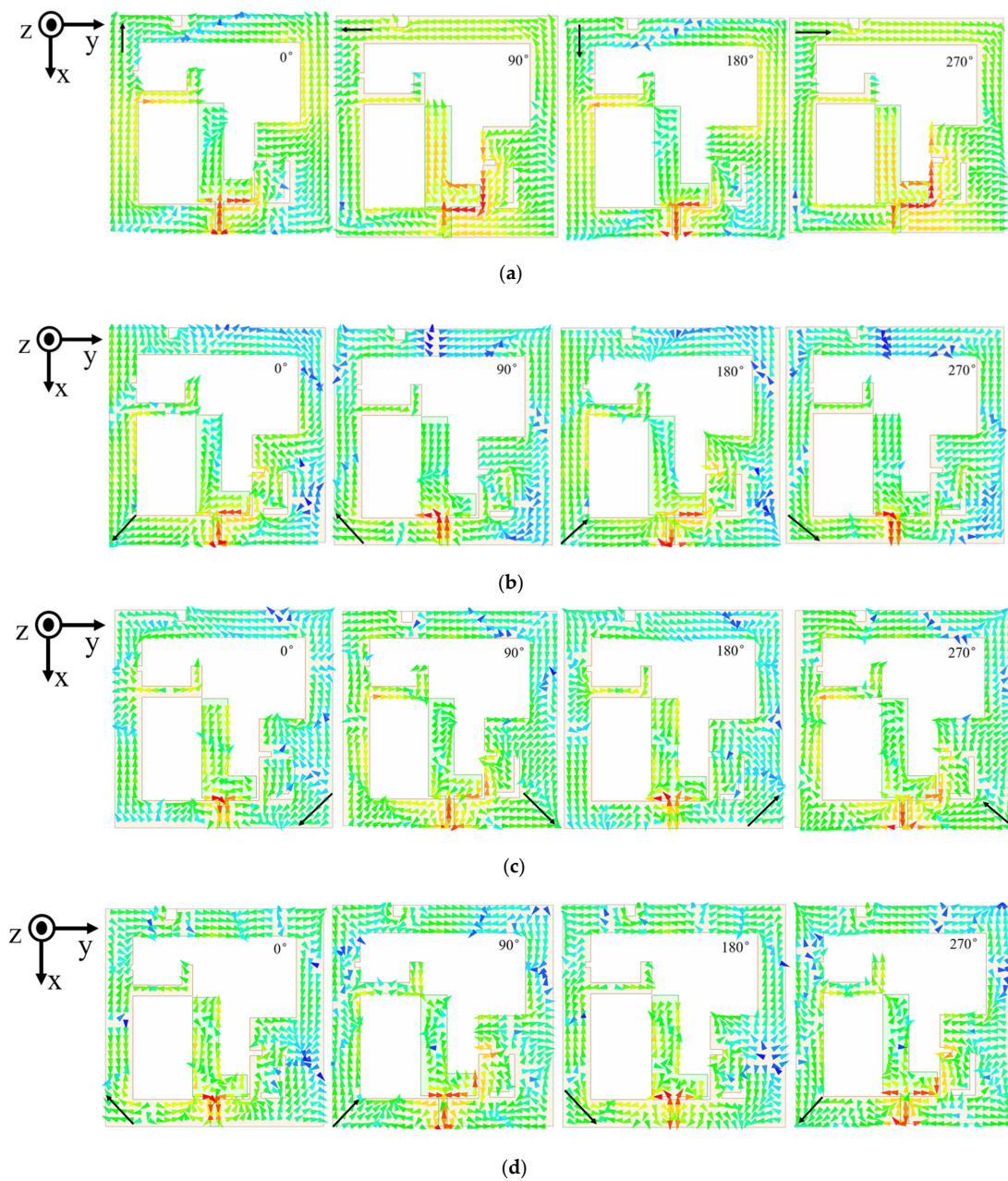


Figure 8. Surface current distributions of the proposed antenna at (a) 1.5 GHz, (b) 4 GHz, (c) 6 GHz, and (d) 7.6 GHz.

The current distributions from 0° to 270° , at 4 GHz, are shown in Figure 8b. The current rotates clockwise with the increasing time phase, and the fields radiated LHCP in the $+Z$ direction. For this frequency, however, most of the currents are located in the area of the L-shaped radiator and the patch on the left bottom corner. There are also some currents

on the top part of the frame. Therefore, there are multi-resonance frequencies in this band, which is consistent with Figure 3.

Figure 8c shows the current distributions from 0° to 270° at 6 GHz. The current rotates counterclockwise with the increasing time phase, and the fields radiated RHCP in +Z direction. However, it has to be mentioned that the 6 GHz band also contains several resonances, and the bandwidth is relatively wide. Several areas contribute to the resultant polarization state. In this sense, this band is affected by several parameters, as discussed in the previous section.

The same observation can be made on the 7.6 GHz band, as seen in Figure 8d. However, the rotational sense is LHCP in the +Z direction. It is interesting to find that the rotational sense changes, alternatingly, with the frequency bands.

5. Measurement and Discussion

The antenna is fabricated using etching technology on an FR4 substrate. The prototype is shown in Figure 9a. The S-parameter is measured by an AV3672D vector network analyzer. The far field and gain are measured in a microwave anechoic chamber, as shown in Figure 9b. The axial ratio is retrieved from the radiation patterns.

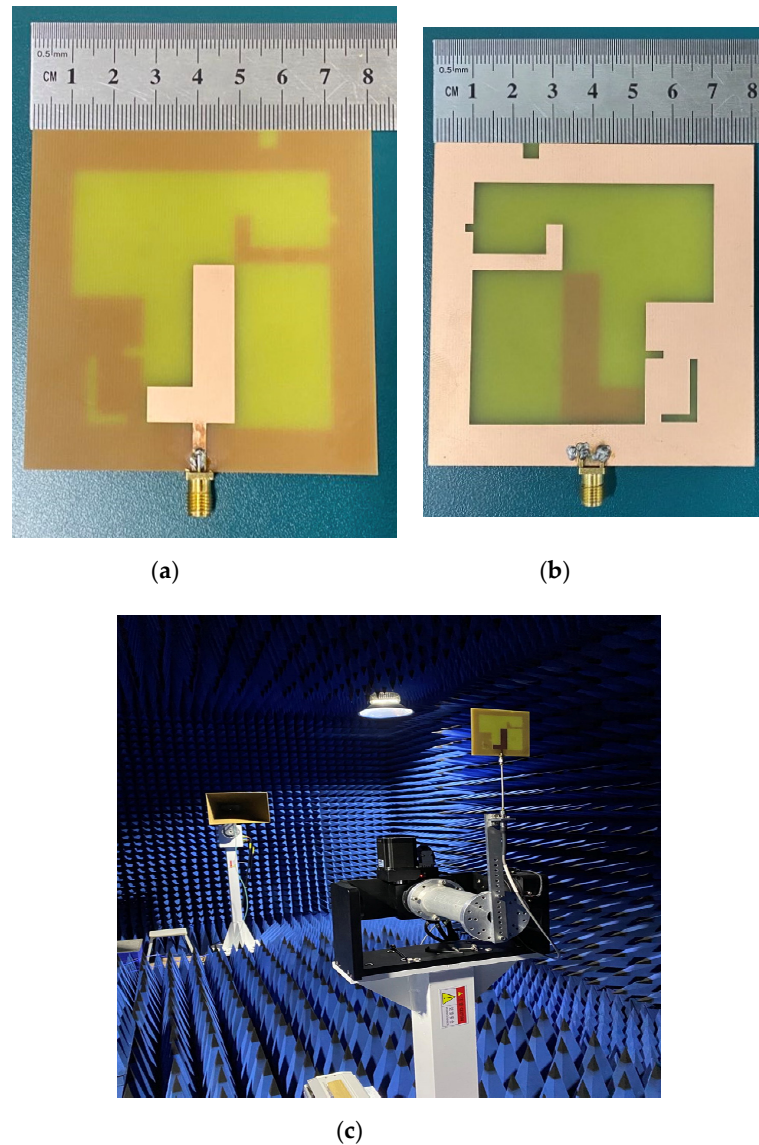


Figure 9. Fabrication and measurement: (a) front view of the proposed antenna; (b) back view of the proposed antenna; (c) far field measurement in an anechoic chamber.

The simulated and measured S parameters, as well as AR, are plotted in Figure 10a,b, respectively. For reflection measurement, the antenna is placed in the anechoic chamber, and the cable is connected to the VNA. Before measurement, the cable is calibrated. As can be seen from the results, four frequency bands have been successfully realized. The -10 dB bandwidths for the four bands are 75.8% (0.95–2.11 GHz), 55.8% (3.05–5.39 GHz), 39.9% (5.84–8.19 GHz), and 10.3% (9.14–10.68 GHz), respectively. The first band covers all four of the navigation systems (1.20 GHz–1.61 GHz). The second band covers several 5G bands. The third and fourth bands are for WIFI-6E and the satellite communication band.

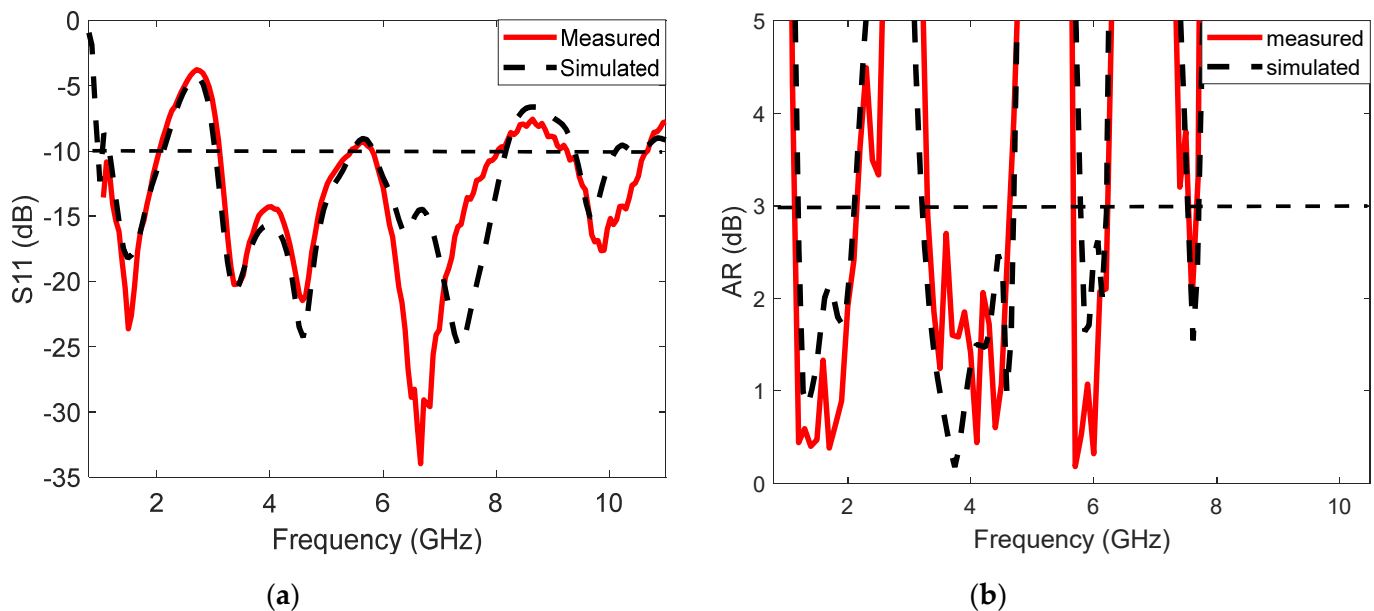


Figure 10. (a) The simulated and measured S11. (b) The simulated and measured AR.

The measured 3 dB bandwidths for AR are 59.4% (1.16–2.14 GHz), 35.8% (3.23–4.64 GHz), 8.4% (5.70–6.20 GHz), and 2.6% (7.51–7.71 GHz). The measured gains are 4.56, 2.28, 4.26, and 4.30 dBi at 1.5 GHz, 3.8 GHz, 6 GHz, and 7.6 GHz, respectively. It can be observed that there is a good agreement between simulated and measured results. The slight difference is mainly due to the soldering error between the SMA connector and the feeder line. At the same time, when performing a far field test, the angle error between the turntables may also affect the test results. The measured results show that the proposed antenna can cover almost all navigation frequency bands, and it can cover 5G, N77, and N78 frequency bands at the same time.

The measured and simulated far-field radiation patterns, in E-plane and H-plane, at 1.5 GHz, 4 GHz, 6 GHz, and 7.6 GHz are plotted in Figure 11. From the radiation patterns, it is clear that the antenna can radiate RHCP at 1.5 GHz, LHCP at 4 GHz, RHCP at 6 GHz, and LHCP at 7.6 GHz in the +z direction. It can also be seen that the antenna radiates a bidirectional wave with the opposite circular polarization. The RHCP is realized in the +z direction, while LHCP is in the $-z$ direction.

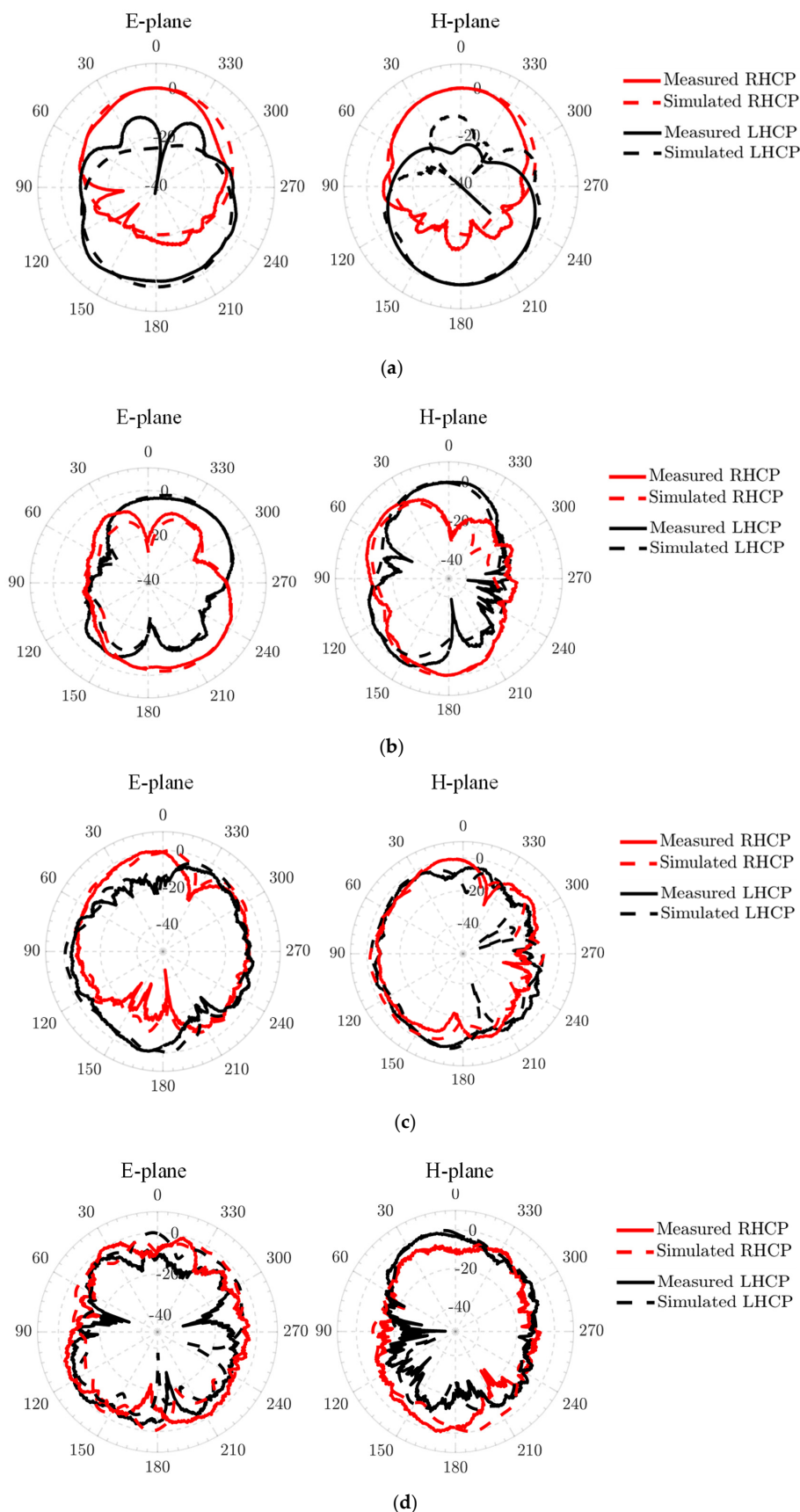


Figure 11. The simulated and measured gain patterns, in E plane and H plane, at (a) 1.5 GHz, (b) 4 GHz, (c) 6 GHz, and (d) 7.6 GHz.

Gain measurement is conducted, by comparison, to standard-gain horn antenna. The measured gain versus the simulated gain is plotted in Figure 12. In the measurement, only the interested bands are measured. It can be seen that the measurement is in satisfactory agreement with the simulation. There are slight differences near 1.5 GHz and 6 GHz. However, the discrepancy is acceptable.

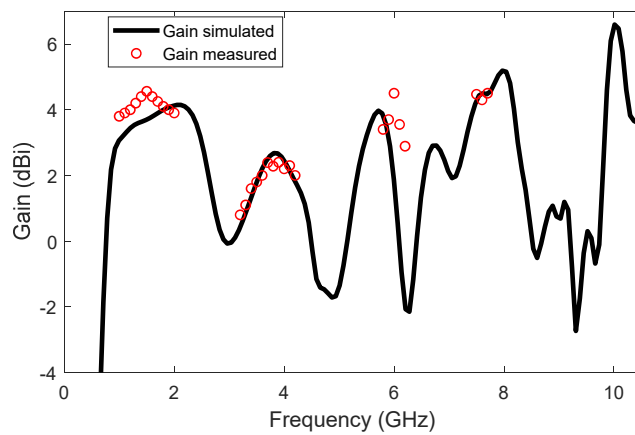


Figure 12. The simulated and measured gain.

A comparison between this work and the designs in the literature is presented in Table 2. Looking at the size of the antenna, this design is moderately large. In terms of operation bands, this work provides four working bands. Particularly, the first three bands have more than 39% relative bandwidths. The first bandwidth is even greater than 75%. Regarding the axial ratio bandwidth, the first band provides a bandwidth of 59.4%, making it the widest design in Table 2. In addition, this design covers all the four navigation systems. Moreover, extra bands can be applied for 5G and WIFI-6E applications. Therefore, this design provides more communication bands with larger bandwidth over an area of moderately large.

Table 2. Comparison of the GNSS CP antennas.

References	Size (mm ³)	Number of Bands	S11 < 10 dB	AR < 3 dB	Applications
[8]	150 × 150 × 18	2	12.7%, 10.1%	3.3%, 3.1%	GPS
[9]	101 × 64 × 1.52	1	86.9%	74.3%	5G, WIFI-6E
[15]	50 × 50 × 5	1	3.2%	1.8%	GPS, GLONASS
[19]	47.7 × 47.7 × 5.8	1	19.7%	13.9%	Telemetry tracking and command system
[22]	93.6 × 96 × 1	2	14.75%, 9.44%	around 2.84GHz, 5.24GHz	WLAN
[23]	130 × 130 × 31.52	2	40.57%	6.56%, 7.74%	GPS
[24]	120 × 120 × 29.6	4	21.1%, 12.8%, 27.1%, 7.5%	11.6%, 7.6%, 7.0%, 7.1%	GPS, BDS, WLAN, Wi-MAX
[25]	35 × 35 × 13.8	3	13.0%, 18.2%, 14.7%	3.53%, 1.73%, 13.62%	Satellite application
[26]	25 × 25 × 1	3	23.4%, 56.5%, 31.14%	10.1%, 4.95%, 10.44%	WLAN/C band X/Ku band
[31]	60 × 60 × 1.0	3	44.0%, 70.9%	35.9%, 44%, 6.3%	WLAN, 5G
This work	80 × 80 × 1.6	4	75.8%, 55.8%, 39.9%, 10.3%	59.4%, 35.8%, 8.4%, 2.6%	GNSS, 5G, WIFI-6E

6. Conclusions

A circularly polarized antenna with simple structure, multiple frequency bands, and a wide axial ratio bandwidth has been presented. The proposed antenna adds an L-shaped

stub and a rectangular patch, on the basis of the L-shaped radiator and rectangular frame, which changes the current distribution by cutting grooves to achieve the superior performance of multiple frequency bands and the wide axial ratio bandwidth. The measured -10 dB bandwidth is 75.8% (0.95–2.11 GHz), 55.8% (3.05–5.39 GHz), 39.9% (5.84–8.19 GHz), and 10.3% (9.14–10.68 GHz), and 3-dB ARBs are 59.4% (1.16–2.14 GHz), 35.8% (3.23–4.64 GHz), 8.4% (5.70–6.20 GHz), and 2.6% (7.51–7.71 GHz). Results show that the antenna can operate in the frequency bands from 1.16 to 2.14 GHz in RHCP for GNSS, from 3.23 to 4.64 GHz in LHCP for 5G, and from 5.925 to 7.125 GHz for WIFI-6E.

Author Contributions: Conceptualization, X.L.; methodology, H.W.; software, X.Y.; validation, J.W.; data curation, H.W.; writing—original draft preparation, H.W.; writing—review and editing, X.L.; funding acquisition, X.L., X.Y. and J.W. All authors have read and agreed to the published version of the manuscript.

Funding: This work is funded in part by the University Synergy Innovation Program of Anhui Province (GXXT-2021-027), the National Natural Science Foundation of China under the contract number of 61871003 and the open project of the state key laboratory of complex electromagnetic environment effects on electronics and information system under grant numbers of CEMEE2022Z0201B, CEMEE2021K0202A.

Conflicts of Interest: The authors declare no conflict of interest.

References

1. Dahri, M.H.; Jamaluddin, M.H.; Khalily, M.; Abbasi, M.I.; Selvaraju, R.; Kamarudin, M.R. Polarization Diversity and Adaptive Beamsteering for 5G Reflectarrays: A Review. *IEEE Access* **2018**, *6*, 19451–19464. [[CrossRef](#)]
2. Tubbal, F.E.; Raad, R.; Chin, K.-W. A Survey and Study of Planar Antennas for Pico-Satellites. *IEEE Access* **2015**, *3*, 2590–2612. [[CrossRef](#)]
3. Chen, X.; Morton, Y.J.; Yu, W.; Truong, T.-K. GPS L1CA/BDS B1I Multipath Channel Measurements and Modeling for Dynamic Land Vehicle in Shanghai Dense Urban Area. *IEEE Trans. Veh. Technol.* **2020**, *69*, 14247–14263. [[CrossRef](#)]
4. Zhong, Z.-P.; Zhang, X.; Liang, J.-J.; Han, C.-Z.; Fan, M.-L.; Huang, G.-L.; Xu, W.; Yuan, T. A Compact Dual-Band Circularly Polarized Antenna With Wide Axial-Ratio Beamwidth for Vehicle GPS Satellite Navigation Application. *IEEE Trans. Veh. Technol.* **2019**, *68*, 8683–8692. [[CrossRef](#)]
5. Feng, G.; Chen, L.; Xue, X.; Shi, X. Broadband Circularly Polarized Crossed-Dipole Antenna With a Single Asymmetrical Cross-Loop. *IEEE Antennas Wirel. Propag. Lett.* **2017**, *16*, 3184–3187. [[CrossRef](#)]
6. Liang, C.-F.; Lyu, Y.-P.; Chen, D.; Cheng, C.-H. Wideband Circularly Polarized Stacked Patch Antenna Based on TM11 and TM10. *IEEE Trans. Antennas Propag.* **2021**. [[CrossRef](#)]
7. Ding, K.; Gao, C.; Yu, T.; Qu, D. Broadband C-Shaped Circularly Polarized Monopole Antenna. *IEEE Trans. Antennas Propag.* **2015**, *63*, 785–790. [[CrossRef](#)]
8. Cai, Y.-M.; Li, K.; Yin, Y.-Z.; Ren, X. Dual-Band Circularly Polarized Antenna Combining Slot and Microstrip Modes for GPS With HIS Ground Plane. *IEEE Antennas Wirel. Propag. Lett.* **2015**, *14*, 1129–1132. [[CrossRef](#)]
9. Le, T.T.; Tran, H.H.; Park, H.C. Simple-Structured Dual-Slot Broadband Circularly Polarized Antenna. *IEEE Antennas Wirel. Propag. Lett.* **2018**, *17*, 476–479. [[CrossRef](#)]
10. Xu, R.; Li, J.-Y.; Yang, J.-J.; Wei, K.; Qi, Y.-X. A Design of U-Shaped Slot Antenna With Broadband Dual Circularly Polarized Radiation. *IEEE Trans. Antennas Propag.* **2017**, *65*, 3217–3220. [[CrossRef](#)]
11. Ellis, M.S.; Zhao, Z.; Wu, J.; Ding, X.; Nie, Z.; Liu, Q.-H. A Novel Simple and Compact Microstrip-Fed Circularly Polarized Wide Slot Antenna With Wide Axial Ratio Bandwidth for C-Band Applications. *IEEE Trans. Antennas Propag.* **2016**, *64*, 1552–1555. [[CrossRef](#)]
12. Rusdiyanto, D.; Zulkifli, F.Y. Dual Band Circularly Polarized Microstrip Antenna Fed By Inverted-L Shaped With A Stub for GPS And WLAN Application. In Proceedings of the 2019 11th International Conference on Information Technology and Electrical Engineering, Pattaya, Thailand, 10–11 October 2019; IEEE: Pattaya, Thailand, 2019; pp. 1–4.
13. Sharma, S.B.; Ugle, A.; Parikh, K. A Novel U-Slot Aperture Coupled Annular-Ring Microstrip Patch Antenna for Multiband GNSS Applications. In Proceedings of the 2020 14th European Conference on Antennas and Propagation, Copenhagen, Denmark, 15–20 March 2020; IEEE: Copenhagen, Denmark, 2020; pp. 1–3.
14. Cao, Y.; Cheung, S.W.; Yuk, T.I. A Simple Planar Polarization Reconfigurable Monopole Antenna for GNSS/PCS. *IEEE Trans. Antennas Propag.* **2015**, *63*, 500–507. [[CrossRef](#)]
15. Yuan, J.; Zheng, J.; Chen, Z.D. A Compact Meandered Ring Antenna Loaded With Parasitic Patches and a Slotted Ground for Global Navigation Satellite Systems. *IEEE Trans. Antennas Propag.* **2018**, *66*, 6835–6843. [[CrossRef](#)]
16. Chen, X.; Fu, G.; Gong, S.-X.; Yan, Y.-L.; Zhao, W. Circularly Polarized Stacked Annular-Ring Microstrip Antenna With Integrated Feeding Network for UHF RFID Readers. *IEEE Antennas Wirel. Propag. Lett.* **2010**, *9*, 542–545. [[CrossRef](#)]

17. Sun, X.; Zhang, Z.; Feng, Z. Dual-Band Circularly Polarized Stacked Annular-Ring Patch Antenna for GPS Application. *IEEE Antennas Wirel. Propag. Lett.* **2011**, *10*, 49–52. [[CrossRef](#)]
18. Yang, H.; Fan, Y.; Liu, X. A Compact Dual-Band Stacked Patch Antenna With Dual Circular Polarizations for BeiDou Navigation Satellite Systems. *IEEE Antennas Wirel. Propag. Lett.* **2019**, *18*, 1472–1476. [[CrossRef](#)]
19. Squadrito, P.; Livreri, P.; Di Donato, L.; Squadrito, C.; Sorbello, G. A Telemetry, Tracking, and Command Antennas System for Small-Satellite Applications. *Electronics* **2019**, *8*, 689. [[CrossRef](#)]
20. Seo, D.C.; Sung, Y. Stacked Open-Loop Square Ring Antenna for Circular Polarization Operation. *IEEE Antennas Wirel. Propag. Lett.* **2015**, *14*, 835–838. [[CrossRef](#)]
21. Yuan, J.; Chen, Z.; Chen, Z.; Li, Y. A Compact Dual-Band Microstrip Ring Antenna Using Multiring Ground for GPS L 1 / L 2-Band. *IEEE Antennas Wirel. Propag. Lett.* **2021**, *20*, 2250–2254. [[CrossRef](#)]
22. Xu, Y.; Zhu, L.; Liu, N.-W. Design Approach for A Dual-Band Circularly Polarized Slot Antenna with Flexible Frequency Ratio and Similar In-Band Gain. *IEEE Antennas Wirel. Propag. Lett.* **2022**. [[CrossRef](#)]
23. Lee, S.; Yang, Y.; Lee, K.-Y.; Hwang, K.C. Dual-Band Circularly Polarized Annular Slot Antenna With a Lumped Inductor for GPS Application. *IEEE Trans. Antennas Propag.* **2020**, *68*, 8197–8202. [[CrossRef](#)]
24. Sharma, A.; Das, G.; Gupta, S.; Gangwar, R.K. Quad-Band Quad-Sense Circularly Polarized Dielectric Resonator Antenna for GPS/CNSS/WLAN/WiMAX Applications. *IEEE Antennas Wirel. Propag. Lett.* **2020**, *19*, 403–407. [[CrossRef](#)]
25. Ameen, M.; Thummaluru, S.R.; Chaudhary, R.K. A Compact Multilayer Triple-Band Circularly Polarized Antenna Using Anisotropic Polarization Converter. *IEEE Antennas Wirel. Propag. Lett.* **2021**, *20*, 145–149. [[CrossRef](#)]
26. Yadav, A.; Singh, V.K.; Yadav, P.; Beliya, A.K.; Bhoi, A.K.; Barsocchi, P. Design of Circularly Polarized Triple-Band Wearable Textile Antenna with Safe Low SAR for Human Health. *Electronics* **2020**, *9*, 1366. [[CrossRef](#)]
27. Li, J.; Shi, H.; Li, H.; Zhang, A. Quad-Band Probe-Fed Stacked Annular Patch Antenna for GNSS Applications. *IEEE Antennas Wirel. Propag. Lett.* **2014**, *13*, 372–375. [[CrossRef](#)]
28. Li, B.; Yang, C.; Yang, Z.; Shi, J.; Li, J.; Zhang, A. Circularly Polarized Array with Enhanced Isolation Using Magnetic Metamaterials. *Electronics* **2019**, *8*, 1356. [[CrossRef](#)]
29. Lai, H.W.; Wong, H. Substrate Integrated Magneto-Electric Dipole Antenna for 5G Wi-Fi. *IEEE Trans. Antennas Propag.* **2015**, *63*, 870–874. [[CrossRef](#)]
30. Syrytsin, I.; Zhang, S.; Pedersen, G.F.; Morris, A.S. User-Shadowing Suppression for 5G Mm-Wave Mobile Terminal Antennas. *IEEE Trans. Antennas Propag.* **2019**, *67*, 4162–4172. [[CrossRef](#)]
31. Xu, R.; Li, J.-Y.; Qi, Y.-X.; Yang, G.-W.; Yang, J.-J. A Design of Triple-Wideband Triple-Sense Circularly Polarized Square Slot Antenna. *IEEE Antennas Wirel. Propag. Lett.* **2017**, *16*, 1763–1766. [[CrossRef](#)]